frontiers | Frontiers in Acoustics

TYPE Original Research
PUBLISHED 20 December 2023
DOI 10.3389/facou.2023.1326759

OPEN ACCESS

EDITED BY
Hyungsuk Lee,
Yonsei University, Republic of Korea

REVIEWED BY
Zhongtao Hu,
Beihang University, China
Claude Inserra,
Université de Lyon, France

*CORRESPONDENCE
James Friend,
jfriend@ucsd.edu
Sreekanth H. Chalasani,
schalasani@salk.edu

†These authors have contributed equally to this work

RECEIVED 23 October 2023
ACCEPTED 23 November 2023
PUBLISHED 20 December 2023

CITATION
Vasan A, Magaram U, Patel J, Friend J and Chalasani SH (2023), Integrating ultrasonic neuromodulation with fiber photometry.
Front. Acoust. 1:1326759.
doi: 10.3389/facou.2023.1326759

Integrating ultrasonic neuromodulation with fiber photometry

Aditya Vasan[1†], Uri Magaram[2,3†], Janki Patel[3], James Friend[1*] and Sreekanth H. Chalasani[3*]

[1]Medically Advanced Devices Laboratory, Department of Mechanical and Aerospace Engineering, Jacobs School of Engineering and Department of Surgery, School of Medicine, University of California San Diego, La Jolla, CA, United States, [2]Neurosciences Graduate Program, University of California San Diego, La Jolla, CA, United States, [3]Molecular Neurobiology Laboratory, The Salk Institute for Biological Studies, La Jolla, CA, United States

Ultrasound has been used to modulate neural activity in rodents and primates; however, combining ultrasound stimulation with *in vivo* imaging in freely moving animals has been challenging. Here, we design and validate a transducer to overcome these challenges in the rodent. We develop a head-mounted ultrasound transducer that can be combined with a fiber photometry system. This combination allows us to monitor ultrasound-evoked responses in striatal neurons in awake and freely moving animals. Together, this system allows for a high-resolution analysis of ultrasound-evoked biology at the level of both neural circuits and behavior in freely moving animals, critical to providing a mechanistic understanding of ultrasound neuromodulation.

KEYWORDS

ultrasound, neuromodulation, fiber photometry, freely moving animals, head-mounted device

Introduction

Ultrasound has been successfully used to modify targets within the mammalian brain. At high intensities, it can ablate tissues (Fry et al., 1955) for treating cancer (Martin et al., 2014) and other neurological conditions like epilepsy (Lipsman et al., 2014; Wang et al., 2015); when combined with contrast agents, it can open the blood-brain-barrier (Hynynen et al., 2005; McDannold et al., 2012) and deliver small molecule drugs (Treat et al., 2007; Alonso et al., 2013) or viral vectors (Alonso et al., 2013). In contrast, ultrasound at lower intensities can directly modulate neuronal activity (Khraiche et al., 2008; Tyler et al., 2008; Tufail et al., 2010). Moreover, ultrasound has been shown to both activate and inhibit neural activity (Bachtold et al., 1998; Lee et al., 2015; Wang et al., 2015; Lee et al., 2016; Legon et al., 2018; Guo et al., 2022), with differential effects on excitatory and inhibitory neurons based on stimulus parameters (Yu et al., 2021). Not surprisingly, the mechanisms underlying *in vivo* ultrasound-evoked neurostimulation remain unclear, but may include thermal- (O'Brien, 2007), mechanical- (Tyler, 2011), auditory- (Guo et al., 2018; Sato et al., 2018), or cavitation-(Plaksin et al., 2014) driven effects. Thus, despite the promise of fully non-invasive ultrasound-based neuromodulation, additional efforts are needed to establish the underlying mechanism, particularly within the mammalian brain.

Electrophysiology, with its excellent temporal resolution, is the preferred method for studying neuronal function (Buzsáki et al., 2012). However, using this method has limited

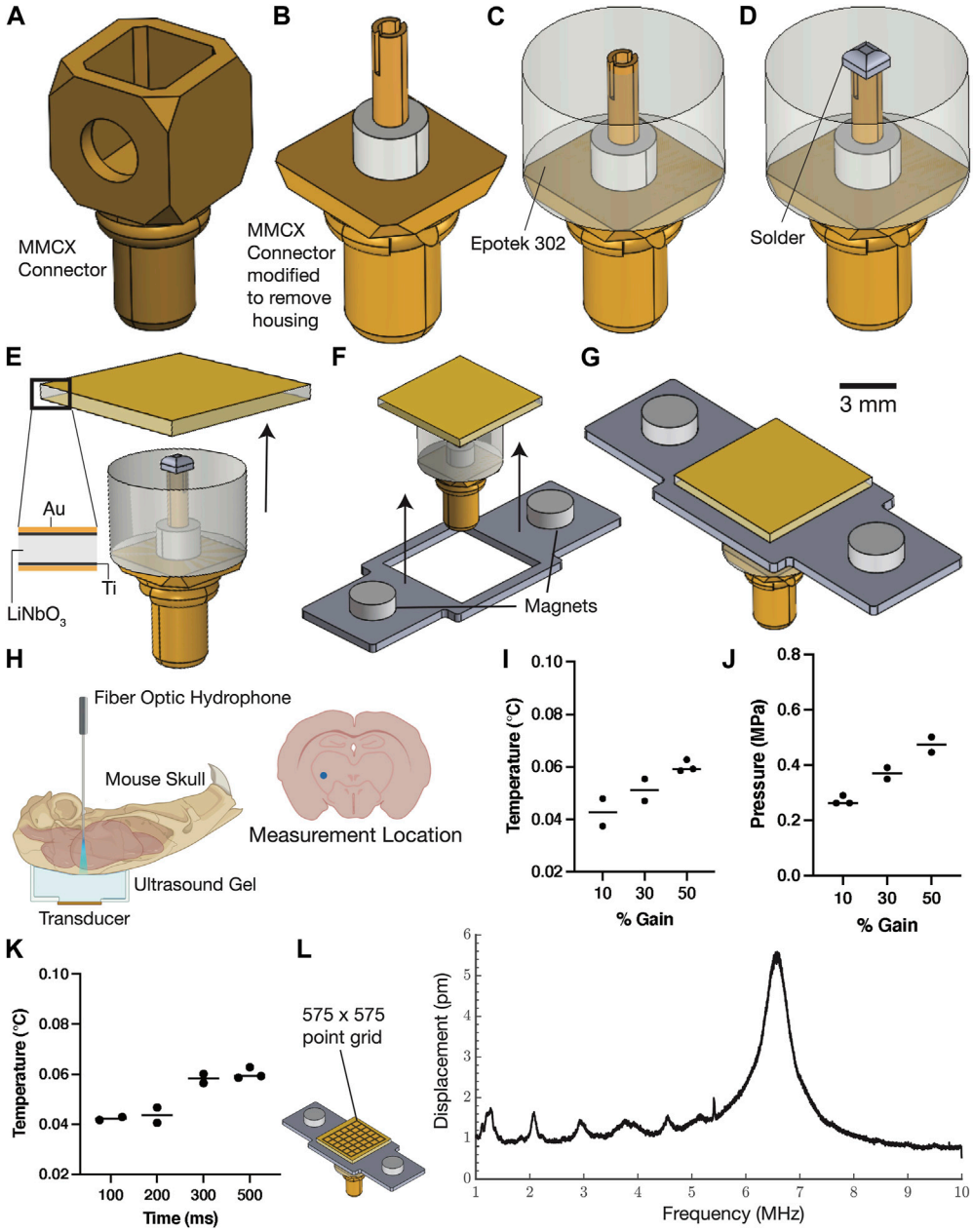

FIGURE 1
Miniature ultrasound transducers for use with freely moving mice. Conventional ultrasound trans-ducers are typically made for imaging and can result in heating or tissue damage when used for cellular stimula-tion. Our device made from single crystalline Lithium Niobate using the manufacturing process described in this figure **(A–G)** can deliver sufficient power through the skull without any significant temperature changes. The device snaps on to a headplate (mounted on the mouse) using magnets and the entire assembly weighs less than a gram. The pressure and temperature were measured using a fiber optic hydrophone in the striatum **(H)** and show signifi-cannot pressure changes for varying input powers to the device **(J)** and insignificant temperature changes **(I–K)**. The vibration amplitude was characterized using a laser doppler vibrometry scan of the transducer face **(L)** and shows the presence of a narrow-band peak centered at 6.5 MHz.

use *in vivo*. While intracellular recordings can be made from a maximum of only a few individual cells (Margrie et al., 2002; Petersen et al., 2003; Chauvette et al., 2010); extracellular recordings measuring activity from multiple cells lack cellular specificity (Buzsáki et al., 2012). Moreover, recording devices for measuring electrical signals from hundreds or thousands of neurons need to be miniaturized to reduce tissue damage (Kim et al., 2013). In contrast, whole-brain imaging techniques, like fMRI, have contributed to understanding how neuronal circuits responding to external stimuli are distributed across large brain regions (Craddock et al., 2013; Van Essen et al., 2013), but have limited spatial and temporal resolution. One solution to these problems is to combine imaging techniques like two-photon microscopy or fiber photometry with fluorescent reporters, where neuronal circuits can be probed at cellular resolution in an intact brain (Grewe and Helmchen, 2009; Grienberger and Konnerth, 2012).

Moreover, genetically encoded calcium indicators can be targeted to specific cell populations, whose activity can then be optically monitored at cellular and even sub-cellular resolution (Helmchen and Denk, 2005; Svoboda and Yasuda, 2006; Göbel et al., 2007).

A common method to monitor fluorescent signals uses an implanted fiber optic cannula (Adelsberger et al., 2005; Lu et al., 2010). Though invasive, this method (fiber photometry) is well-suited to record neural activity across cell populations in freely-moving animals (Martianova et al., 2019). In addition, fiber photometry can also be used to record signals from multiple locations in the rodent brain (Kim et al., 2016; Sych et al., 2019). Moreover, the result is an aggregate of calcium changes from many neurons that cannot be easily resolved, but provides a complementary approach to microendoscopic or two-photon imaging (Jennings et al., 2015). Combining ultrasound stimulation with this imaging method would provide insights into the mechanisms underlying ultrasound-evoked neuromodulation.

Here, we develop a new, lightweight ultrasound transducer that can be mounted on the head of a freely moving animal and integrate this device with a fiber photometry system. This setup allows us to monitor calcium signals from striatal neurons in moving animals upon ultrasound stimulation.

Results

A new ultrasound transducer for modulating neural activity in freely moving mice

Most ultrasound applications use lead zirconate titanate (PZT) transducers, which are prone to heating and hysteresis at higher frequencies (Morozov et al., 2005). In contrast, transducers made from lithium niobate have been shown to have minimal heating and no hysteresis at frequencies typically used for neuromodulation (Nakamura and Shimizu, 1989; Collignon et al., 2018). We started with a micro-miniature coaxial swivel connector (MMCX, Figure 1A) and exposed the central pin and surrounding ceramic insulation using a Dremel benchtop drill (Figure 1B). Next, we added a layer of backing epoxy (Epotek 302, Epoxy Technologies Inc., Billerica, United States of America) onto the modified connector, leaving the lead tip exposed (Figure 1C). We fabricated a lithium niobate transducer (see Methods for details) and soldered it to the device to establish an electrical contact (Figure 1E). This device uses a custom-designed magnetic connector to attach to a matching plate on the animal's head. The magnetic connector is designed to slide onto the device and is anchored in place using a backing epoxy (Figure 1F). The final assembly (Figure 1G) mass is ~0.6 g and was characterized for its pressure outputs in an *ex vivo* preparation as previously described (Figure 1H (Vasan et al., 2022)). Ultrasound has been shown to cause heating in target tissues (O'Brien, 2007). We monitored the temperature rise in the striatum using a fiber optic hydrophone and found that the change in temperature did not exceed 0.1°C (Figure 1I) during use. In addition, we found that the pressure through the intact skull was between 0.3–0.5 MPa (Figure 1K). We also analyzed the vibrational characteristics of this device using laser Doppler vibrometry and found that the fundamental thickness mode's resonance frequency was 6.56 MHz (Figure 1L). This device was then used in combination with fiber photometry probes as described in later sections for analysis of neural activity in freely moving animals.

Stereotactic placement of the device on the head of an adult mouse

Previous studies have shown that ultrasound stimulation can evoke neuronal activity in both cortex and hippocampus (Tufail et al., 2010), but have yet to assess this in more ventral regions of the brain. To assess the feasibility of ultrasound stimulation in freely moving mice, the device was attached to a headplate mounted to the skull with dental cement and a fiber optic cannula was implanted to target the dorsal striatum using stereotactic coordinated (Murphy et al., 2022). To test whether a sparse population of neurons could be stimulated, we expressed a genetically encoded calcium indicator, GCaMP6s, in cholinergic neurons, which constitute about 2% of neurons in the dorsal striatum (Zhou et al., 2002). We mounted a ChAT::CRE transgenic mouse on a stereotax under anesthesia (Figure 2A) and injected a floxed virus expressing GCaMP6s (Figure 2B) using a calibrated nanoliter injection system (Nanoject II). The head plate was affixed to the device and the assembly was lowered over the injection site (Figure 2D). Next, the head plate was anchored in place using dental cement (Figures 2E, F). We then dried the exposed area and implanted a fiber optic cannula as previously described (Hollon et al., 2021; Dong et al., 2022). Finally, the scalp was sutured, and additional ultraviolet curable dental cement was used to firmly affix the head plate (Figures 2H, I). Mice were allowed to recover for two to 4 weeks prior to conducting studies with the head-mounted transducer.

Assessing locomotor behavior with head-mounted transducer

To determine whether locomotor behaviors are affected by the presence of the ultrasound transducer, mice of several genotypes were assessed in rotarod (Figure 3A) and open-field assays (Figure 3C). Control mice, untethered by the transducer and cables, stayed on the rotarod an average of 53.6 s (± 6.9 s SEM), and an average of 63.2 s (± 3.9 s SEM) when connected via magnet and cables to the transducer (Figure 3B). These results did not reach significance in either direction, indicating that the presence of the tethered transducer did not affect the ability of the mice to maintain their coordination on the rotarod. In open-field assays, ambulatory behaviors measured by average distance and velocity in both the first 5 minutes (Figures 3D, E) and 45 min (Figures 3F, G) did not change significantly in the presence of the transducer either, indicating that the head-mounted transducer design is compatible with freely-moving mouse behavior and assays.

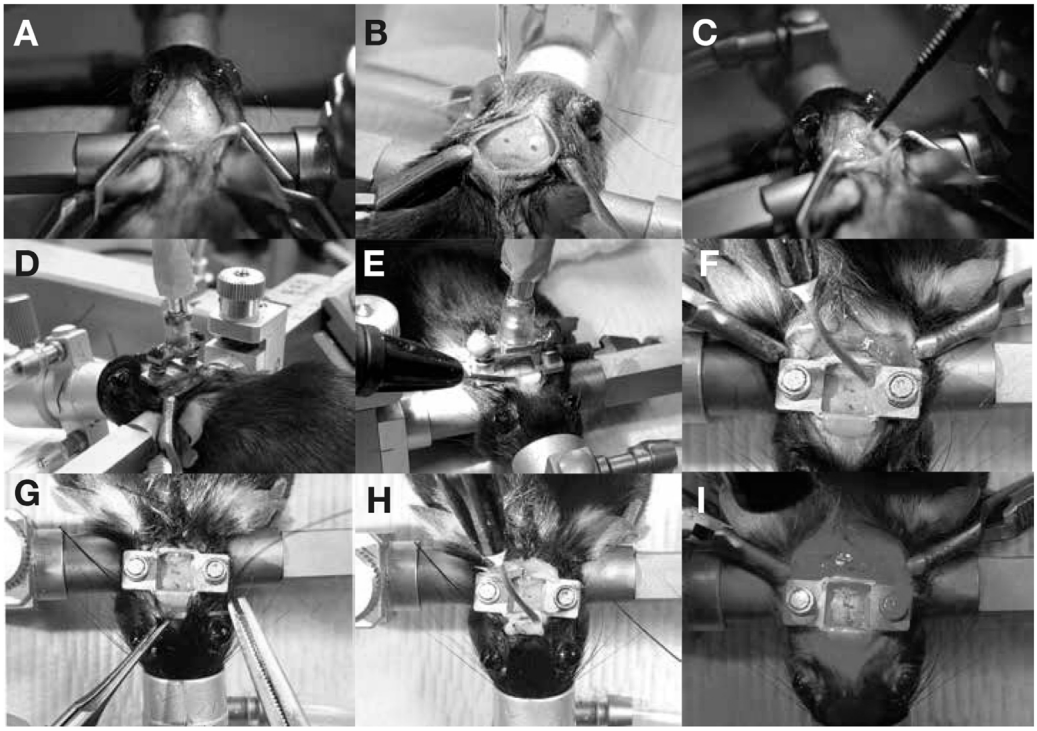

FIGURE 2
Device implant procedure. Mice are anesthetized using isoflurane and mounted on a stereotax. An incision is made to expose the skull **(A)** and the bregma and lambda structures were identified to perform virus injections **(B)**. The area was cleaned with cotton swabs **(C)** and the MMCX device-headplate assembly was lowered over the injection site **(D,E)**. The headplate was affixed using UV-curable dental cement **(F)** and additional implants (such as fiberphotometry cannulas) were implanted at this stage. The scalp was sutured **(G)** and additional dental cement was dispensed **(H)** at this stage if needed. The exposed skull **(I)** was cleaned using hydrogen peroxide and cotton swabs before returning the mouse to its cage.

Ultrasound-evoked activation of striatum in freely moving mice

We used fiber photometry recordings to test whether transcranial ultrasound could evoke calcium activity in freely moving animals. After recovery from the protocol described above (Figure 4), mice were attached to the ultrasound delivery and fiber photometry systems (Figure 4A). We first confirmed that the fiber optic cannula was placed into the dorsal striatum and GCaMP6s expression was restricted to cholinergic neurons in the striatum (Figure 4B). All animals (N = 5) showed significant increases in cholinergic calcium activity upon ultrasound stimulation compared to controls (Figures 4C, D). Together, these results show that the custom-designed ultrasound device is capable of delivering sufficiently powerful ultrasound to endogenously activate striatal cholinergic neurons in an awake, freely moving animal, while avoiding the hindering of the animal's movement in an open field or upon a rotating rod.

Discussion

We demonstrate the development of a novel method for integrating ultrasound neuromodulation tools with well-established readout techniques for neuronal activity. Specifically, we develop a new head-mounted transducer that can be combined with a fiber photometry system to stimulate striatal neurons in a freely moving mice. We designed, fabricated, and tested a small lightweight transducer that can be mounted on the head of freely moving mice. Although there are other works that use head-mounted transducers (Murphy et al., 2022; Yang et al., 2023), they have used lower frequencies, higher pressure inputs and do not present validation of the devices with rotarod and open field tests. This device can deliver stimuli with 0.3–0.5 MPa peak negative pressure in a deep brain region, the dorsal striatum. The mechanical index for the parameters listed in this study is 0.19, well below the U.S Federal Drug Administration's mandated clinical safety threshold of 1.9 for bubble-free tissue, and is half the threshold for bubble-laden tissue (Nelson et al., 2009; Church et al., 2015). These parameters are thus unlikely to cause cavitation in tissue and do not affect cell viability. Further, the frequency used in this study is well outside the hearing threshold for mice (1–100 kHz) (Heffner and Heffner, 2007). Specifically, we show that we can activate calcium activity in cholinergic neurons without hindering the animal's ability to explore freely or grasp a rotating rod. Moreover, the ultrasound transducer can be removed from the head plates (these are attached using a magnetic connector), allowing the animals to be returned to their home cages and be repeatedly tested, as is commonly done in most striatal-driven behaviors (Balleine et al., 2007; Lipton et al., 2019). We used fiber photometry as a readout of ultrasound-evoked neuromodulation, however, recent studies have shown that these

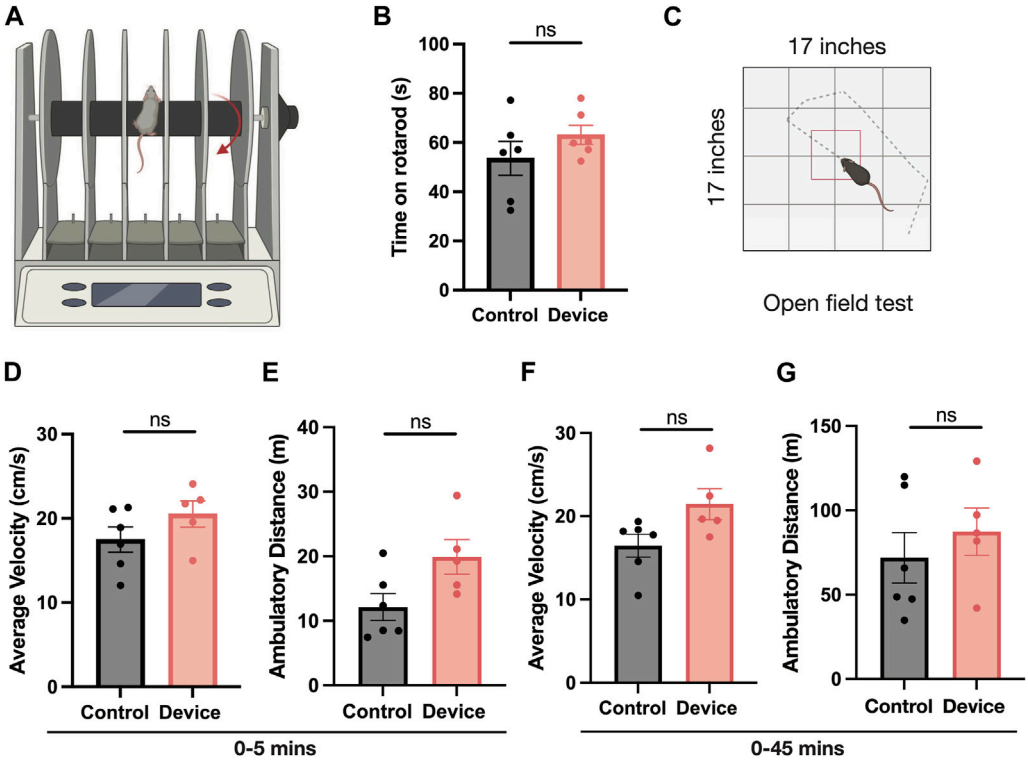

FIGURE 3
Asessing mobility of animal with head-mounted transducer. **(A,B)** Rotarod and **(C–G)** open field tests were conducted to assess mobility of the animal with the device. Mice outfitted with the wearable ultrasound device (red) show no reduction (N = 6, Mann-Whitney test) in ability to stay on the rotor rod (schematic, **(A)** as measured by time spent on rotarod over three trials compared to naive controls (gray) with no device **(B)**. In open field testing **(D–G)**, mice connected to the wearable ultrasound device (red) display no reduced locomotion as measured by average velocity in the first 5 minutes, total distance convered in the first 5 minutes, average velocity over 45 min, or total distance covered over 45 min (N = five to six, Mann Whitney test).

data primarily reflect non-somatic changes in calcium and might not correspond to spiking-related activity (Legaria et al., 2022). Consistently, we suggest that our device can be used to modify neuronal calcium levels in striatal neurons. More broadly, we suggest that this device can be combined with mouse genetics to probe the ultrasound and sonogenetic control of neuronal circuits and behaviors. Collectively, our system can be used to provide mechanistic insights into how ultrasound affects specific neuronal circuits and their associated behaviors.

Materials and methods

Animals

Animals used in this study were group housed in an American Association for the Accreditation of Laboratory Animal Care approved vivarium on a 12 h light/dark cycle, and all protocols were approved by the Institutional Animal Care and Use Committee of the Salk Institute for Biological Studies. C57BL/6 mice (JAX 000664), aged 10–14 weeks were used to measure ultrasound pressures *in vivo*. ChAT-Cre mice aged P22 and older were used for fiber photometry experiments. The mice were free to move when the ultrasound stimulus reported in this study was delivered.

Ex vivo hydrophone measurements

Hydrophone measurements were performed with a fiber-optic hydrophone (FOHS92, Precision Acoustics, Dorchester, UK) *ex vivo*. C57BL/6 mice (JAX 000664), aged 10–14 weeks, were sacrificed and decapitated. The skin over the skull was removed, followed by removal of the lower mandible, soft palate and hard palate. Once the ventral part of the brain was exposed, the mouse head preparation was placed dorsal side down on the diffuser assembly coupled with ultrasound gel, and the hydrophone tip was lowered into the ventral portion of the brain using a micromanipulator. Data from measurements made on at least three animals is shown.

Fiber photometry

A commercially available fiber photometry system (FP3002, Neurophotometrics, San Diego, CA) was used to measure calcium activity *in vivo*. Briefly, recordings were done by alternating 473 nm and 415 nm excitation light at 80 Hz, for a total of 40 Hz recordings in calcium dependent GCaMP6s and isosbestic (calcium independent) channels, respectively. Excitation power was adjusted to provide 50 µW of light at the tip of the patch cord, calibrated with a fiber optic power meter (PM20A, Thor Labs,

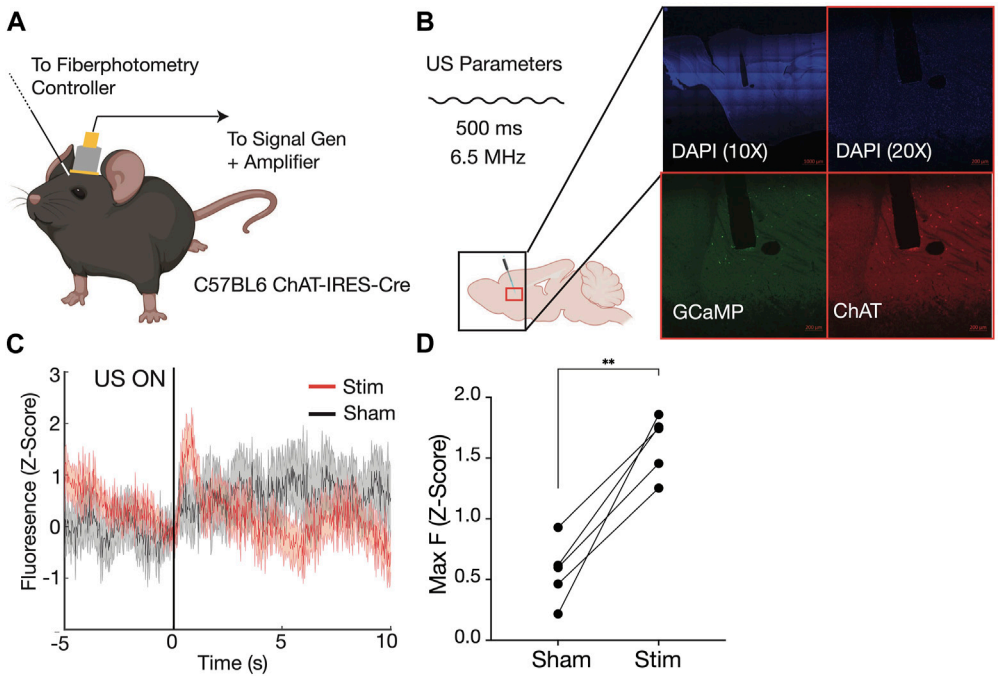

FIGURE 4
Simultaneous fiber photometry recordings and transcranial ultrasound stimulation in awake, freely moving mouse. Schematic of recording setup **(A)**, with fiber photometry cannula implanted anterior to magnetic headplate holding custom built 6.56 MHz ultrasound transducer on head of CHAT-IRES-Cre mouse. Immunofluoresence confirms fiber photometry cannula (white dotted line) in dorsal striatum, as well as GCAMP6s expression in ChAT+ cells of the striatum **(B)**. Sample average trace of ultrasound ON trials (red) compared to ultrasound OFF (sham control) trials (gray) aligned to onset of ultrasound at time 0 **(C)** shows increased fluoresence under stimulation. Maximum GCAMP6s fluorescence in ultrasound trials (Stim) is significantly higher than in Sham conditions across five mice, calculated in the 3-s window after stimulus delivery **(D)**.

Newton, NJ). For anesthetized recordings with the larger device, mice were anesthetized and held at 1% isoflurane, adjusted as needed to maintain sedation on the stereotactic frame without abolishing all measurable brain activity. The skin over the skull was removed and the transducer coupled to the skull with ultrasound gel. For awake, behavior-based recordings, the mouse was anesthetized to allow for careful attachment of the fiber optic cable. After the head-mounted device was attached via magnets and coupled with ultrasound gel, the mouse was allowed to wake up in its home cage, and ultrasound stimulations were delivered interspersed with control pulses.

Immunohistochemistry

Immunofluorescence was collected from free-floating 50 µm sections after extended (3 days) fixation in 4% paraformaldehyde or 10% formalin for better visualization of cannula lesion. Sections were blocked at room temperature for 1 h in blocking buffer (0.25% Triton-X and 5% donkey serum in 1x phosphate buffered saline (PBS). Up to three of the following primary antibodies were then applied for incubation in blocking buffer overnight at 4°C: chicken or rabbit polyclonal GFP (1:250 Aves GFP-1020 or ThermoFisher A6455, respectively) for labelling GCaMP6s positive neurons, goat polyclonal ChAT (1:250 EMD Millipore, AB144P) for labelling cholinergic neurons, and chicken polyclonal Parvalbumin (1:250 Encor Biotech, CPCA-PvalB) for labeling PV-interneurons. Following primary antibody incubation, sections were washed three times for 5 min each in PBS to reduce non-specific antibody binding effects. Secondary antibodies conjugated to fluorophores 488, 594, or 647 raised in donkey or goat (1:500) were applied for 3 hours at room temperature in blocking buffer. Nuclei were stained with DAPI (1:1000 ThermoFisher D1306) before washing sections three times in PBS for 5 min each. Sections were mounted on slides with a coverslip using ProLong Gold Antifade Mountant (P10144, ThermoFisher, Waltham, MA) and allowed to dry for 24 h before confocal imaging (LSM 880, Zeiss, Oberkochen, Germany).

Rotarod assay

ChAT-Cre mouse locomotor behaviour was evaluated on a Rotor-Rod (SD Instruments, San Diego, CA). Mice underwent a single day of training at a constant speed of 4 RPM for 3 min to acclimate to the Rotor-Rod. The next day, mice were placed on a rod that started at 0 RPM and gradually increased to 30 RPM over a 5-min period. The latency to fall off the rod was collected. Each mouse underwent 4 trials daily with a 20-min inter-trial interval in which mice were returned to their cages. The latency to fall off was averaged across the three best trials. This procedure was repeated across 5 days. The experimenter was blinded as to the identity of groups.

Ultrasound transducers

Single-crystal lithium niobate transducers operating in the fundamental thickness mode with lateral dimensions of 5 x 5 mm and a thickness of 500 μm were used in this study. The 128YX cut of lithium niobate was used and the fabrication process involved cleaning of the wafer with acetone, isopropyl alcohol, and ultra-pure deionized (DI) water followed by sputtering both sides with an adhesion layer of 20 nm titanium followed by 1 μm gold. The 36YX cut is typically recommended for thickness-mode transducers, but in low-loss, narrowband applications, it has been found that the 128YX cut produces superior coupling and output amplitude (Collignon et al., 2018). The deposition parameters were (with a Denton Discovery 635, Denton Vacuum LLC, New Jersey, United States of America) 5–10 nm of Ti at 1.2–1.6 A/s with the power set to 200W, with argon as the gas in the chamber at 2.3 mT and the stage rotating at 13RPM to ensure uniform deposition over the sample. The thickness of gold deposited was 1 μm at a rate of 7–9 A/s. Devices using the LN elements were driven using a waveform generator (33600 A, Keysight Inc, Santa Rosa, CA) and amplifier (VTC2057574, Vox Technologies, Richardson, TX), and input power was measured using an oscilloscope (Infiniivision MSOX 2024A, Keysight) mated to voltage (N2862B, Keysight) and current probes (CT1, Tektronix, Beaverton, OR) connected as near to the transducer as practicable. The gain on the amplifier was varied to adjust the pressure and the control pulses were run at zero amplifier gain during trials.

Open field

In the open field test, a 17″ x 17″ x 12” (Med Associates Inc., Fairfax, VT) was used to test the Locomotor abilities of mice. ChAT-Cre, DAT-Cre, or wildtype mice were placed in the center of the arena and their movement was tracked for 45 min. In test mice, head transducer was attached to the headplate, and the wires were threaded through a commutator to avoid tangles. The commutator was secured to a flexible arm above the arena and stabilized with a sturdy plank. If the transducer wires got tangled, the recording was paused, and the transducer was readjusted before resuming. 16- beam IR arrays along the *X* and *Y*-axis of the arena tracked the position of the mouse. Activity monitor software was used to analyze the average velocity and distance travelled in 60 s bins. Average velocity and distance travelled was calculated for the first 5 min and for the entire 45 min for each mouse. One device mouse lost device for 2 out of 45 min and one control mouse was removed for negligible ambulation.

Viral injections and implants

Intracranial injections were performed in a surgery work area under aseptic conditions. Mice were anesthetized via 5% isoflurane induction and held at 1% isoflurane (Somnosuite Kent Scientific, Torrington, CT) throughout surgery on a heating pad and stereotactic frame. After shaving and sterilization, a midline incision into skin to expose the skull was made, and the skull was leveled.

For cannula and head plate implantation, the skull was dried and primed with OptiBond primer (KerrDental, Orange, CA). A small craniotomy was made using a surgical drill (1.25 mm diameter) at the appropriate coordinates. Injections into dorsal striatum were made using a Nanoject III (Drummond Scientific, Broomall, PA) via glass micropipette loaded with virus. Virus was injected at 3 nL/s with 1 s pause until total volume was injected. The micropipette was withdrawn 10 min after full volume of virus was injected, after which a 200 μm fiber optic cannula (Neurophotometrics, San Diego, CA) was lowered into dorsal striatum 5 μm above the injection site. Using a minimal amount of light-curable dental cement, the cannula was affixed in place to the skull to provide maximal exposed skull for subsequent ultrasound experiments.

For behavior experiments, a custom-designed head plate was also affixed to the skull using dental cement just ventral to the cannula leaving the central portion of skull exposed.

Following surgery, the skin was either closed where possible via suture (AD Surgical, Sunnyvale, CA) or VetBond (3M, Two Harbors, MN). Mice were injected with buprenorphine (1 mg/kg) and monitored for at least 3 days post-surgery.

Injections were performed unilaterally into dorsal striatum using coordinates +1.0 AP, −2.3 ML, −3.5 DV for vertical injections and +1.7 AP, −2.3 ML, −3.5 DV for injections at 15* on AP axis when leaving more room for head plate for a total of 300 nL. AAV9 hSyn.GCaMP6s.WPRE.SV40 (Addgene #100843-AAV9) was injected at 1e13 into WT mice and AAV9 Syn.Flex.GCaMP6s.WPRE.SV40 (Addgene #100845-AAV9) was injected into ChAT$^{IRES-Cre}$ mice.

Data availability statement

The raw data supporting the conclusion of this article will be made available by the authors, without undue reservation.

Ethics statement

The animal study was approved by the Institutional Animal Care and Use Committee of the Salk Institute for Biological Studies (protocol No. 15-00064, 10/25/2021). The study was conducted in accordance with the local legislation and institutional requirements.

Author contributions

AV: Conceptualization, Formal Analysis, Investigation, Methodology, Validation, Visualization, Writing–original draft. UM: Conceptualization, Formal Analysis, Investigation, Methodology, Validation, Visualization, Writing–original draft. JP: Investigation, Writing–original draft. JF: Conceptualization, Data curation, Funding acquisition, Investigation, Methodology, Project administration, Resources, Supervision, Writing–review and editing. SC: Conceptualization, Data curation, Funding acquisition, Investigation, Methodology, Project administration, Resources, Supervision, Writing–review and editing.

Funding

The author(s) declare financial support was received for the research, authorship, and/or publication of this article. This work was supported by funds from the W. M. Keck Foundation (JF), Brain Research Foundation (JF), NIH R01NS115591 (SC and JF), and MH111534 (SC).

Acknowledgments

We are grateful to the prototyping lab at the Qualcomm Institute and Steve Barry (Salk Machine Shop) for their help with fabricating the components of the MMCX devices and head plates, respectively. We would also like to thank Sage Aronson, PhD (Neurophotometrics LLC.), and Nick Hollon, PhD for their support in setting up fiberphotometry experiments. We thank members of the JF and SC labs for critical help, advice and inputs.

Conflict of interest

The authors declare that the research was conducted in the absence of any commercial or financial relationships that could be construed as a potential conflict of interest.

The author(s) declared that they were an editorial board member of Frontiers, at the time of submission. This had no impact on the peer review process and the final decision.

Publisher's note

References

Adelsberger, H., Garaschuk, O., and Konnerth, A. (2005). Cortical calcium waves in resting newborn mice. *Nat. Neurosci.* 8, 988–990. doi:10.1038/nn1502

Alonso, A., Reinz, E., Leuchs, B., Kleinschmidt, J., Fatar, M., Geers, B., et al. (2013). Focal delivery of AAV2/1-transgenes into the rat brain by localized ultrasound-induced BBB opening. *Mol. Therapy-Nucleic Acids* 2, e73. doi:10.1038/mtna.2012.64

Bachtold, M. R., Rinaldi, P. C., Jones, J. P., Reines, F., and Price, L. R. (1998). Focused ultrasound modifications of neural circuit activity in a mammalian brain. *Ultrasound Med. Biol.* 24, 557–565. doi:10.1016/s0301-5629(98)00014-3

Balleine, B. W., Delgado, M. R., and Hikosaka, O. (2007). The role of the dorsal striatum in reward and decision-making: figure 1. *J. Neurosci.* 27, 8161–8165. doi:10.1523/jneurosci.1554-07.2007

Buzsáki, G., Anastassiou, C. A., and Koch, C. (2012). The origin of extracellular fields and currents—EEG, ECoG, LFP and spikes. *Nat. Rev. Neurosci.* 13, 407–420. doi:10.1038/nrn3241

Chauvette, S., Volgushev, M., and Timofeev, I. (2010). Origin of active states in local neocortical networks during slow sleep oscillation. *Cereb. cortex* 20, 2660–2674. doi:10.1093/cercor/bhq009

Church, C. C., Labuda, C., and Nightingale, K. (2015). A theoretical study of inertial cavitation from acoustic radiation force impulse imaging and implications for the mechanical Index1. *Ultrasound Med. Biol.* 41, 472–485. doi:10.1016/j.ultrasmedbio.2014.09.012

Collignon, S., Manor, O., and Friend, J. (2018). Improving and predicting fluid atomization via hysteresis-free thickness vibration of lithium niobate. *Adv. Funct. Mater.* 28, 1704359. doi:10.1002/adfm.201704359

Craddock, R. C., Jbabdi, S., Yan, C. G., Vogelstein, J. T., Castellanos, F. X., Di Martino, A., et al. (2013). Imaging human connectomes at the macroscale. *Nat. methods* 10, 524–539. doi:10.1038/nmeth.2482

Dong, A., He, K., Dudok, B., Farrell, J. S., Guan, W., Liput, D. J., et al. (2022). A fluorescent sensor for spatiotemporally resolved imaging of endocannabinoid dynamics *in vivo*. *Nat. Biotechnol.* 40, 787–798. doi:10.1038/s41587-021-01074-4

Fry, W. J., Fry, F., Barnard, J., Krumins, R., and Brennan, J. (1955). Ultrasonic lesions in the mammalian central nervous system. *Science* 122, 517–518. doi:10.1126/science.122.3168.517

Göbel, W., Kampa, B. M., and Helmchen, F. (2007). Imaging cellular network dynamics in three dimensions using fast 3D laser scanning. *Nat. methods* 4, 73–79. doi:10.1038/nmeth989

Grewe, B. F., and Helmchen, F. (2009). Optical probing of neuronal ensemble activity. *Curr. Opin. Neurobiol.* 19, 520–529. doi:10.1016/j.conb.2009.09.003

Grienberger, C., and Konnerth, A. (2012). Imaging calcium in neurons. *Neuron* 73, 862–885. doi:10.1016/j.neuron.2012.02.011

Guo, H., Hamilton, M., Offutt, S. J., Gloeckner, C. D., Li, T., Kim, Y., et al. (2018). Ultrasound produces extensive brain activation via a cochlear pathway. *Neuron* 98, 1020–1030.e4. doi:10.1016/j.neuron.2018.04.036

Guo, H., Offutt, S. J., Hamilton II, M., Kim, Y., Gloeckner, C. D., Zachs, D. P., et al. (2022). Ultrasound does not activate but can inhibit *in vivo* mammalian nerves across a wide range of parameters. *Sci. Rep.* 12, 2182–2214. doi:10.1038/s41598-022-05226-7

Heffner, H. E., and Heffner, R. S. (2007). Hearing ranges of laboratory animals. *J. Am. Assoc. Lab. Anim. Sci.* 46, 20–22.

Helmchen, F., and Denk, W. (2005). Deep tissue two-photon microscopy. *Nat. methods* 2, 932–940. doi:10.1038/nmeth818

Hollon, N. G., Williams, E. W., Howard, C. D., Li, H., Traut, T. I., and Jin, X. (2021). Nigrostriatal dopamine signals sequence-specific action-outcome prediction errors. *Curr. Biol.* 31, 5350–5363.e5. doi:10.1016/j.cub.2021.09.040

Hynynen, K., McDannold, N., Sheikov, N. A., Jolesz, F. A., and Vykhodtseva, N. (2005). Local and reversible blood–brain barrier disruption by noninvasive focused ultrasound at frequencies suitable for trans-skull sonications. *Neuroimage* 24, 12–20. doi:10.1016/j.neuroimage.2004.06.046

Jennings, J. H., Ung, R., Resendez, S., Stamatakis, A., Taylor, J., Huang, J., et al. (2015). Visualizing hypothalamic network dynamics for appetitive and consummatory behaviors. *Cell* 160, 516–527. doi:10.1016/j.cell.2014.12.026

Khraiche, M. L., Phillips, W. B., Jackson, N., and Muthuswamy, J. (2008). "Ultrasound induced increase in excitability of single neurons," in 2008 30th Annual International Conference of the IEEE Engineering in Medicine and Biology Society, Vancouver, BC, Canada, August, 2008, 4246–4249.

Kim, C. K., Yang, S. J., Pichamoorthy, N., Young, N. P., Kauvar, I., Jennings, J. H., et al. (2016). Simultaneous fast measurement of circuit dynamics at multiple sites across the mammalian brain. *Nat. methods* 13, 325–328. doi:10.1038/nmeth.3770

Kim, T.-i., McCall, J. G., Jung, Y. H., Huang, X., Siuda, E. R., Li, Y., et al. (2013). Injectable, cellular-scale optoelectronics with applications for wireless optogenetics. *Science* 340, 211–216. doi:10.1126/science.1232437

Lee, W., Kim, H., Jung, Y., Song, I. U., Chung, Y. A., and Yoo, S. S. (2015). Image-guided transcranial focused ultrasound stimulates human primary somatosensory cortex. *Sci. Rep.* 5, 8743. doi:10.1038/srep08743

Lee, W., Kim, H. C., Jung, Y., Chung, Y. A., Song, I. U., Lee, J. H., et al. (2016). Transcranial focused ultrasound stimulation of human primary visual cortex. *Sci. Rep.* 6, 34026. doi:10.1038/srep34026

Legaria, A. A., et al. (2022). Fiber photometry in striatum reflects primarily nonsomatic changes in calcium. *Nat. Neurosci.* 1-5.

Legon, W., Bansal, P., Tyshynsky, R., Ai, L., and Mueller, J. K. (2018). Transcranial focused ultrasound neuromodulation of the human primary motor cortex. *Sci. Rep.* 8, 10007. doi:10.1038/s41598-018-28320-1

Lipsman, N., Mainprize, T. G., Schwartz, M. L., Hynynen, K., and Lozano, A. M. (2014). Intracranial applications of magnetic resonance-guided focused ultrasound. *Neurotherapeutics* 11, 593–605. doi:10.1007/s13311-014-0281-2

Lipton, D. M., Gonzales, B. J., and Citri, A. (2019). Dorsal striatal circuits for habits, compulsions and addictions. *Front. Syst. Neurosci.* 13, 28. doi:10.3389/fnsys.2019.00028

Lutcke, H., Murayama, M., Hahn, T., Margolis, D. J., Astori, S., Zum Alten Borgloh, S. M., et al. (2010). Optical recording of neuronal activity with a genetically-encoded calcium indicator in anesthetized and freely moving mice. *Front. Neural Circuits* 4, 9. doi:10.3389/fncir.2010.00009

Margrie, T. W., Brecht, M., and Sakmann, B. (2002). *In vivo*, low-resistance, whole-cell recordings from neurons in the anaesthetized and awake mammalian brain. *Pflügers Arch.* 444, 491–498. doi:10.1007/s00424.002.0831.z

Martianova, E., Aronson, S., and Proulx, C. D. (2019). Multi-fiber photometry to record neural activity in freely-moving animals. *JoVE J. Vis. Exp.*, e60278. doi:10.3791/60278

Martin, E., et al. (2014). Clinical neurological HIFU applications: the Zurich experience. *Transl. Cancer Res.* 3, 449–458.

McDannold, N., Arvanitis, C. D., Vykhodtseva, N., and Livingstone, M. S. (2012). Temporary disruption of the blood–brain barrier by use of ultrasound and microbubbles: safety and efficacy evaluation in rhesus macaques. *Cancer Res.* 72, 3652–3663. doi:10.1158/0008-5472.can-12-0128

Morozov, M., Damjanovic, D., and Setter, N. (2005). The nonlinearity and subswitching hysteresis in hard and soft PZT. *J. Eur. Ceram. Soc.* 25, 2483–2486. doi:10.1016/j.jeurceramsoc.2005.03.086

Murphy, K. R., Farrell, J. S., Gomez, J. L., Stedman, Q. G., Leung, S. A., et al. (2022). A tool for monitoring cell type-specific focused ultrasound neuromodulation and control of chronic epilepsy. *Proc. Natl. Acad. Sci. U. S. A.* 119, e2206828119. doi:10.1073/pnas.2206828119

Nakamura, K., and Shimizu, H. (1989). Hysteresis-free piezoelectric actuators using LiNbO3 plates with a ferroelectric inversion layer. *Ferroelectrics* 93, 211–216. doi:10.1080/00150198908017348

Nelson, T. R., Fowlkes, J. B., Abramowicz, J. S., and Church, C. C. (2009). Ultrasound biosafety considerations for the practicing sonographer and sonologist. *J. Ultrasound Med.* 28, 139–150. doi:10.7863/jum.2009.28.2.139

O'Brien, W. D., Jr. (2007). Ultrasound-biophysics mechanisms. *Prog. Biophys. Mol. Biol.* 93, 212–255. doi:10.1016/j.pbiomolbio.2006.07.010

Petersen, C. C., Hahn, T. T., Mehta, M., Grinvald, A., and Sakmann, B. (2003). Interaction of sensory responses with spontaneous depolarization in layer 2/3 barrel cortex. *Proc. Natl. Acad. Sci.* 100, 13638–13643. doi:10.1073/pnas.2235811100

Plaksin, M., Shoham, S., and Kimmel, E. (2014). Intramembrane cavitation as a predictive bio-piezoelectric mechanism for ultrasonic brain stimulation. *Phys. Rev. X* 4, 011004. doi:10.1103/physrevx.4.011004

Sato, T., Shapiro, M. G., and Tsao, D. Y. (2018). Ultrasonic neuromodulation causes widespread cortical activation via an indirect auditory mechanism. *Neuron* 98, 1031–1041.e5. doi:10.1016/j.neuron.2018.05.009

Svoboda, K., and Yasuda, R. (2006). Principles of two-photon excitation microscopy and its applications to neuroscience. *Neuron* 50, 823–839. doi:10.1016/j.neuron.2006.05.019

Sych, Y., Chernysheva, M., Sumanovski, L. T., and Helmchen, F. (2019). High-density multi-fiber photometry for studying large-scale brain circuit dynamics. *Nat. methods* 16, 553–560. doi:10.1038/s41592-019-0400-4

Treat, L. H., McDannold, N., Vykhodtseva, N., Zhang, Y., Tam, K., and Hynynen, K. (2007). Targeted delivery of doxorubicin to the rat brain at therapeutic levels using MRI-guided focused ultrasound. *Int. J. cancer* 121, 901–907. doi:10.1002/ijc.22732

Tufail, Y., Matyushov, A., Baldwin, N., Tauchmann, M. L., Georges, J., Yoshihiro, A., et al. (2010). Transcranial pulsed ultrasound stimulates intact brain circuits. *Neuron* 66, 681–694. doi:10.1016/j.neuron.2010.05.008

Tyler, W. J. (2011). Noninvasive neuromodulation with ultrasound? A continuum mechanics hypothesis. *Neuroscientist* 17, 25–36. doi:10.1177/1073858409348066

Tyler, W. J., Tufail, Y., Finsterwald, M., Tauchmann, M. L., Olson, E. J., and Majestic, C. (2008). Remote excitation of neuronal circuits using low-intensity, low-frequency ultrasound. *PloS one* 3, e3511. doi:10.1371/journal.pone.0003511

Van Essen, D. C., Smith, S. M., Barch, D. M., Behrens, T. E., Yacoub, E., and Ugurbil, K. (2013). The Wu-Minn human connectome project: an overview. *Neuroimage* 80, 62–79. doi:10.1016/j.neuroimage.2013.05.041

Vasan, A., Allein, F., Duque, M., Magaram, U., Boechler, N., Chalasani, S. H., et al. (2022). Microscale concert Hall Acoustics to produce uniform ultrasound stimulation for targeted sonogenetics in hsTRPA1-transfected cells. *Adv. NanoBiomed Res.* 2, 2100135. doi:10.1002/anbr.202100135

Wang, T. R., Dallapiazza, R., and Elias, W. J. (2015). Neurological applications of transcranial high intensity focused ultrasound. *Int. J. Hyperth.* 31, 285–291. doi:10.3109/02656736.2015.1007398

Yang, Y., Yuan, J., Field, R. L., Ye, D., Hu, Z., Xu, K., et al. (2023). Induction of a torpor-like hypothermic and hypometabolic state in rodents by ultrasound. *Nat. Metab.* 5, 789–803. doi:10.1038/s42255-023-00804-z

Yu, K., Niu, X., Krook-Magnuson, E., and He, B. (2021). Intrinsic functional neuron-type selectivity of transcranial focused ultrasound neuromodulation. *Nat. Commun.* 12, 2519. doi:10.1038/s41467-021-22743-7

Zhou, F. M., Wilson, C. J., and Dani, J. A. (2002). Cholinergic interneuron characteristics and nicotinic properties in the striatum. *J. Neurobiol.* 53, 590–605. doi:10.1002/neu.10150